J Bionic Eng 17 (2020) 695–707
DOI: https://doi.org/10.1007/s42235-020-0062-z

Journal of Bionic Engineering
http://www.springer.com/journal/42235

Redundancy in Biology and Robotics: Potential of Kinematic Redundancy and its Interplay with Elasticity

Tom Verstraten[1*], Christian Schumacher[2], Raphaël Furnémont[1], Andre Seyfarth[2], Philipp Beckerle[3,4]

1. *Robotics and Multibody Mechanics Research Group* (*R&MM*), *Vrije Universiteit Brussel and Flanders Make*, *Pleinlaan* 2, 1050 *Elsene*, *Belgium*
2. *Institute of Sports Science*, *TU Darmstadt*, *Magdalenenstraße* 27, 64289 *Darmstadt*, *Germany*
3. *Elastic Lightweight Robotics Group*, *Robotics Research Institute*, *TU Dortmund*, *Otto-Hahn-Straße* 8, 44227 *Dortmund*, *Germany*
4. *Institüt fur Mechatronische Systeme im Maschinenbau*, *TU Darmstadt*, *Otto-Berndt-Straße* 2, 64287 *Darmstadt*, *Germany*

Abstract

Redundancy facilitates some of the most remarkable capabilities of humans, and is therefore omni-present in our physiology. The relationship between redundancy in robotics and biology is investigated in detail on the Series Elastic Dual-Motor Actuator (SEDMA), an actuator inspired by the kinematic redundancy exhibited by myofibrils. The actuator consists of two motors coupled to a single spring at the output. Such a system has a redundant degree of freedom, which can be exploited to optimize aspects such as accuracy, impedance, fault-tolerance and energy efficiency. To test its potential for human-like motions, the SEDMA actuator is implemented in a hopping robot. Experiments on a physical demonstrator show that the robot's movement patterns resemble human squat jumps. We conclude that robots with bio-inspired actuator designs facilitate human-like movement, although current technical limitations may prevent them from reaching the same dynamic and energetic performance.

Keywords: bioinspired, redundant actuation, series elastic actuation, hopping robots, energy efficiency, human physiology

1 Introduction

Since Raibert presented his well-known work on legged robots[1], a remarkable amount of research on hopping and jumping robots has been published[2,3]. Vertical hopping, as a simple dynamic motion task, can provide understanding of biological concepts of locomotion, *e.g.*, by template models[4,5]. The interest in this topic is explained by the fact that the repulsive, spring-like leg function in vertical hopping can be seen as a subtask of legged locomotion[6]. In robotics, hopping can be used as a basis for the development of new hardware and control designs.

Despite years of research, the agility and versatility with which humans and animals are able to move, is still unrivaled by current state-of-the-art robotic systems[7]. Inspired by biology, series springs have been implemented in several hopping and jumping robots[7–10] in an attempt to close the gap. The spring's function is to store and release energy during repulsive hopping cycles. Using the elasticity of the tendons and aponeuroses, the hopping motion – and locomotion in general – can be performed in a much more energy-efficient way[11–13]. It is well-known that elastic tissues play a crucial role and shape the characteristics of jumping motions[14,15].

Another explanation for the exceptional capabilities of humans is the fact that our physiology as well as our motor control system incorporates redundancy on multiple levels. It therefore comes as no surprise that redundancy has also been applied in several actuators and robots performing human-like tasks. Research in robotics has shown that redundancy can improve precision[16], enlarge the operating range of the actuator[17,18] or the workspace of the robot[19], increase efficiency of the robot[20–22] or the individual actuators[23–25], improve dynamic interaction[26–28] or provide safety[29]. In this work, we will focus on kinematic redundancy on a motor-level, which is present in biology in the construction of myofibril within the human muscle. The

***Corresponding author:** Tom Verstraten
E-mail: Tom.Verstraten@vub.be

potential of this type of redundancy for bio-inspired motion in robotics is what we will explore in this work.

The basis of our study is the kinematically redundant Dual-Motor Actuator (DMA) which was introduced in Ref. [24]. To create a closer match with biology, a series elastic element is added to this actuator, creating a novel concept which we coin the Series Elastic Dual-Motor Actuator (SEDMA)[30]. The SEDMA has tremendous potential for reducing the energy consumption of actuators performing typical human motions: simulations presented in Ref. [30] indicate that a 16% reduction in energy consumption can be achieved by replacing the series elastic actuator of an active ankle prosthesis by a SEDMA. In this work, the SEDMA's ability to perform energy-efficient bio-inspired motion is verified in hardware by implementing it in a robotic demonstrator: a robot consisting of a two-link segmented leg with actuated knee, performing low-frequency squat jumps. High-level control of the SEDMA is achieved by the biomimetic Virtual Model Control[31], using the well-known Spring-Loaded Inverted Pendulum (SLIP) model[5] as a basis. The controller also incorporates an actuator-specific low-level control algorithm for the SEDMA, which was introduced and discussed in Ref. [32].

The aim of this work is to assess the potential of combining series elasticity with kinematically redundant actuation for energy-efficient, bio-inspired motion in robotics, taking into account practical limitations of such a design. The contributions of the work are twofold. First, the performance of the hopping robot driven by the SEDMA actuator and the bio-inspired controller is compared to the human leg and its biomechanics. This comparison reveals interesting similarities between the robotic implementation and its biological counterpart, but also highlights limitations arising from the specific mechanical implementation. Second, the paper presents test results on the SEDMA which are critically analyzed in terms of energy consumption, relating its performance to the design parameters. The analysis leads to the interesting insight that the interplay between the DMA and the spring could result in decreased performance of the system in the presence of friction.

2 Demonstrator

2.1 SEDMA

A schematic of the SEDMA is depicted in Fig. 1. It consists of a DMA combined with a series spring. Series elasticity can bring many benefits to robots, *e.g.* intrinsic safety and cheap force sensing capabilities[33]. Here, the main purpose of the spring is to protect the DMA's planetary differential from the impacts at touchdown, which can be several times higher than the robot's weight[34]. Furthermore, the spring can reduce the work required from the motor by absorbing energy during knee flexion and re-injecting it during the extension phase of the jump.

The DMA is described in detail in Ref. [24]. It consists of two drivetrains coupled to a planetary differential, constructed out of a 10: 1 Neugart PLFE 064 planetary gearbox. The sun gear is driven by a 150 W Maxon RE40 DC motor with a planetary gear reducer of ratio 15: 1, and the ring gear by a 200 W Maxon EC-4pole motor, with a 15: 1 reduction provided by a planetary gearbox and an additional 3: 1 reduction provided by a spur gear pair. The output of the planetary differential is the carrier, just like in an ordinary planetary gearbox.

The series elastic element is an extension spring with a stiffness of 19.87 $N \cdot mm^{-1}$. An item KGT 20 × 20 spindle gear (gear ratio 314 $rad \cdot m^{-1}$, efficiency 85%) converts the rotary output motion of the DMA into a linear displacement of the spring.

All relevant specifications of the hopping robot and its drivetrain are listed in Tables 1 and 2. Friction coefficients were obtained experimentally in prior work[24]. As shown in Ref. [28], the proposed model of the DMA provides a very good fit to dynamic measurements.

2.2 MARCO Hopper II

The MARCO Hopper II test bench on which the SEDMA was implemented is depicted in Fig. 2. The setup, introduced in Ref. [35], represents a human leg with an actuated knee. The robotic leg is approximately half the size of the human leg, and weights of the individual parts were chosen to resemble the mass distribution in the human body[36]. Two links of equal length (l_l = 250 mm) and mass (m_l = 0.17 kg) correspond

Table 1 Specifications of the planetary differential

Parameters	Value
Gear ratio	9: 1
Efficiency of planetary differential	88%
Inertia of the output (carrier)	$12e^{-2}$ kg·m²
Carrier viscous friction	$1e^{-3}$ N·m·(rad·s^{-1})$^{-1}$
Coulomb friction of output (carrier)	0.1033 N·m

Table 2 Specifications of the drivetrains of which the DMA is composed

Parameters	Sun drivetrain	Ring drivetrain
Drivetrain inertia	$1.6e^{-5}$ kg·m^2	$4.9e^{-6}$ kg·m^2
Viscous friction coefficient	$1.5e^{-5}$ N·m·(rad·s^{-1})$^{-1}$	$1.5e^{-12}$ N·m·(rad·s^{-1})$^{-1}$
Coulomb friction coefficient	0.0080 N·m	0.0061 N·m
Motor	Maxon RE40	Maxon EC-4pole 30
Nominal power	150 W	200 W
Nominal torque	177 mN·m	135 mN·m
Maximum speed	12 000 rpm	25 000 rpm
Terminal resistance	0.299 Ohm	0.102 Ohm
Torque constant	30.2 mN·m·A^{-1}	13.6 mN·m·A^{-1}
Gearbox	Maxon GP42	Maxon GP42
Gear ratio	91/6	91/6
Gearbox efficiency	81%	81%

to the shank and thigh. A mass of $m_H = 1.8$ kg is attached to the hip joint in order to mimic the trunk; a mass of $m_F = 0.30$ kg represents the foot. A cable between the trunk mass and foot has two functions: It prevents overextension of the knee, but also transfers kinetic energy from the trunk to the foot, aiding the foot to leave the ground. Furthermore, the trunk and foot are mounted on a linear bearing to ensure a purely vertical motion.

The leg is actuated through a Bowden cable, connected to a pulley (radius 4.3 cm) at the knee joint (mass $m_K = 0.23$ kg). With this configuration, only an extension torque can be applied to the knee – flexion torques are not required for hopping to match to the SLIP model[5]. The other end of the Bowden cable is connected to the series spring of the SEDMA, described previously.

The robot is equipped with Bürster potentiometers (S/N 8709-5250) measuring the distance between the hip and foot, as well as the position of the foot relative to the ground. The extension of the spring is measured with another Bürster potentiometer (S/N 8709-5150). A SCAIME ZF100 sensor is used to sense the force in the Bowden cable. Finally, the position and speed of the spindle is inferred from the two incremental encoders (500 CPT) on the motors of the SEDMA.

2.3 Control

The control framework, depicted schematically in Fig. 3, was presented in previous work[32]. In this section, we only give a condensed overview of the control strategy.

The high-level controller is implemented as a state machine, which distinguishes between the flight phase and the stance phase. In the flight phase, the robot is allowed to move freely in the air, and the commanded force is zero. As soon as the leg reaches a certain minimum length, the stance phase is initiated. At this point, the hopper is controlled by means of Virtual Model Control (VMC)[31]. In this control strategy, the commanded spring force is calculated by replacing the dynamics of the robot with that of a single-mass harmonic oscillator. It is commonly accepted that this model, known as the Spring-Loaded Inverted Pendulum (SLIP) model, describes the dynamics of running and hopping well[5]. In previous work, the VMC-based control strategy was successfully applied to the MARCO Hopper II with a traditional motor-gearbox as actuator[35,37] and with the SEDMA[32]. The approach was also proven to be successful on other robotic legs, *e.g*. Ref. [38].

The mass m_v of the virtual harmonic oscillator is set to 1 kg, leaving the virtual stiffness k_v to determine the hopping pattern. According to Ref. [35], the minimum virtual stiffness required for hopping is:

$$k_v > \frac{2m_v g}{l_0 - x_0} = 140 \ \text{N·m}^{-1}$$

where $x_0 = 26$ cm is the length of the virtual spring at its maximum compression and $l_0 = 40$ cm is the maximum (extended) length of the virtual spring. In our experiments, we met this requirement by choosing $k_v = 175$ N·m^{-1}.

The force control is performed with a cascaded controller, consisting of an inner speed loop and an outer force loop. A crucial part of the speed control loop is the control allocator, whose purpose is to translate the desired output speed to a set of motor speeds. The solution chosen by the control allocator is the one which leads to a minimal electrical energy consumption. In practice, however, it is hard to achieve this optimal speed distribution at all times due to the dynamics of the system[32]. Finally, the low-level controller converts the desired

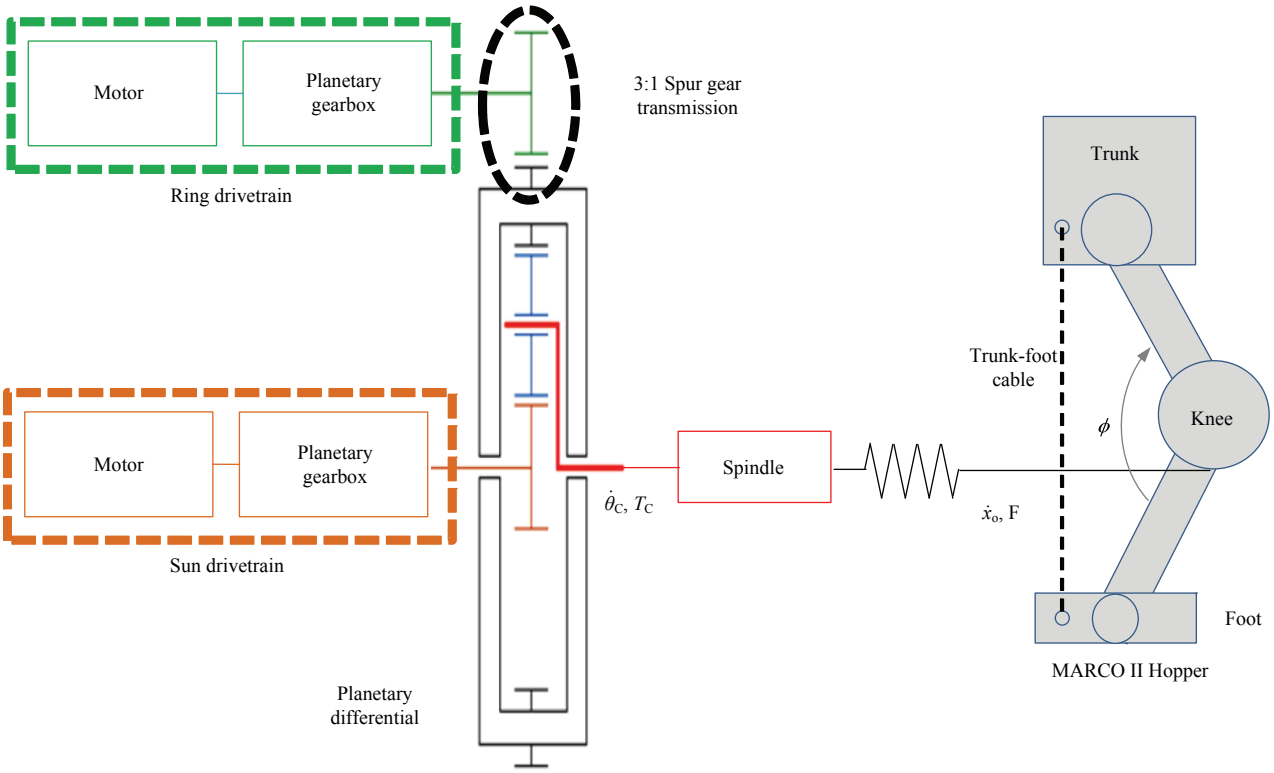

Fig. 1 Schematic of the SEDMA and the MARCO Hopper II.

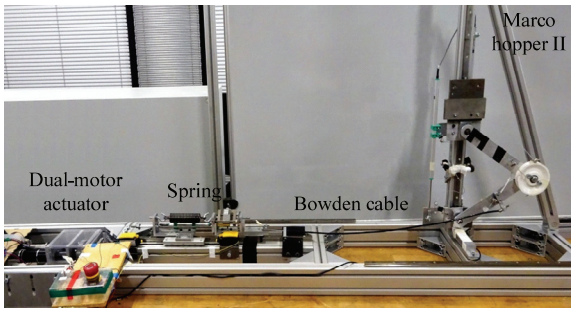

Fig. 2 The SEDMA on the MARCO Hopper II setup.

motor speeds to the required currents for both motors. These currents are used as set points for the Maxon EPOS3 drives in the sun and ring branch, which are both operated in Cyclic Synchronous Torque (CST) mode.

3 Experiments

In this section, we present experiments on the Marco Hopper II actuated by the SEDMA. We start by discussing the hopping pattern generated by the bio-inspired virtual model control. Next, we analyze the force-length characteristic of the hopper and the workloops of the SEDMA. Finally, the energy-efficiency of the actuator is discussed.

3.1 Hopping pattern

Fig. 4 shows the first ten seconds of a hopping trial, which is also shown in the video added as supplementary file to this manuscript. A constant hopping height of 24 mm could be achieved after only a short transient. This height is in line with the experiments previously presented by Oehlke *et al.*[35], although the hopping frequency is lower (1.02 Hz compared to 1.5 Hz). This is due to limitations in the actuator's bandwidth resulting from high friction and its interplay with elasticity, as explained in section **4.2**. An important difference between the work by Oehlke *et al*. and this work is the way how friction is compensated. In Ref. [35], this is done by increasing the virtual spring stiffness during the upward motion. As a result, the resulting energy injection may be higher than strictly needed for compensating the friction, and lead to an increase in hopping frequency. In this work, friction is compensated through a friction model, so that the injected energy corresponds to the actual energy lost during the motion.

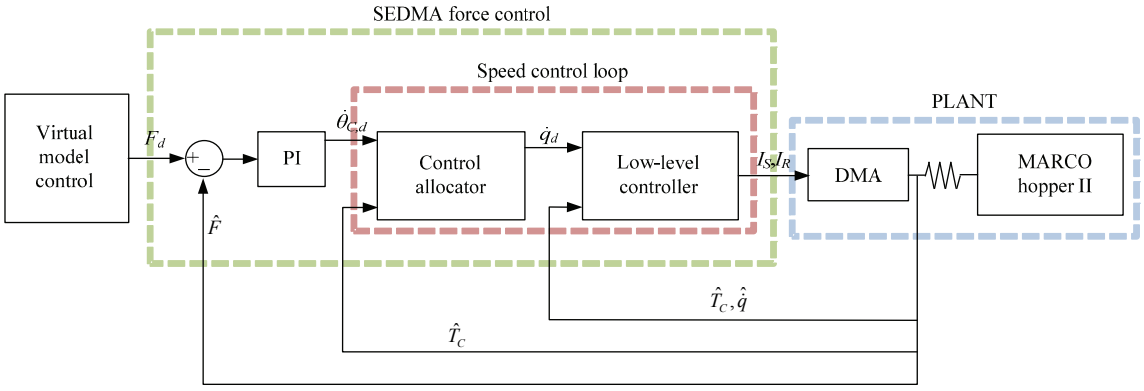

Fig. 3 Control schematic.

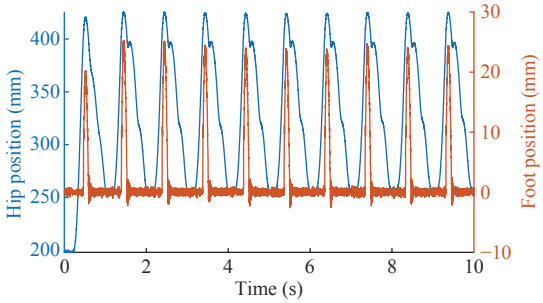

Fig. 4 Foot and hip position for the MARCO Hopper II. Hopping is initiated from a squat position (hip height 200 mm), meaning that the virtual spring is loaded at the beginning of the trial. After a short transient, the hopping height converges to a constant value of 24 mm, at a hopping frequency of 1.02 Hz.

3.2 Force-length characteristic of virtual leg spring

In section **2.3**, we explained that the controller was designed upon the assumption that the dynamics of the hopping robot resemble those of a single-mass harmonic oscillator. To verify to what extent the hops are truly spring-like, we estimated the ground reaction force based on the acceleration of the hopper's center of mass and plotted this force as a function of the compression of the virtual leg spring (Fig. 5). In contrast to what one would expect at hopping frequencies preferred by human subjects, the relationship is very non-linear and definitely not spring-like. The force profile exhibits a peak force at minimal compression, *i.e.* when the leg reaches maximum extension. This force occurs due to the engagement of a mechanical end stop at the knee, which prevents it from extending above 165°. The engagement of this knee stop results in an impulsive force, seen in the estimated ground reaction force. A second peak force, which occurs halfway through the downward motion, is less easily explained. There is no force in the Bowden cable at this point in time, nor is there a clear relationship with the kinematics of the jumping motion. It must however be noted that a similar force peak is observed in data from human low-frequency jumps, as we will discuss in section **4.2**. Finally, friction forces, which are not accounted for in this estimation, explain the negative force at the end of the upward motion and the onset of the swing phase.

3.3 Workloop analysis

In order to study the contribution of different elements or the whole leg, workloop analyses are a common tool in biomechanics[39–42]. For the Marco Hopper II, the workloop of the load side encloses a big area in which positive energy is generated in the system (grey area in Fig. 6, total energy 8.5 J). This is due to the hopping pattern, as no active cable pull is generated during the compression phase. Here, the friction of the system (*e.g.* friction in bearings) dissipates energy in order to decelerate the leg.

Around mid-stance, the actuator starts pulling in order to create an extension knee torque. In this phase, most of the energy is generated. The inertia of the drivetrain and the delayed detection of the flight state cause a prolonged knee extension, such that the cable force rises when the leg is already leaving the ground. This can explain the different shape of the hopper's actuator work loop compared to simulation models of hopping[42] and long jumping[39], both with a similar leg and muscle-tendon unit structure. Due to the deflection of the spring, the motor side of the spindle has to move over a

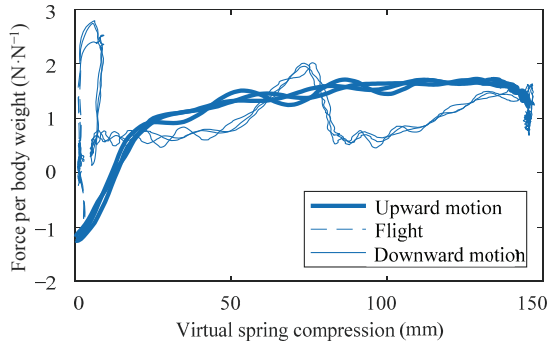

Fig. 5 Force-length characteristic of the virtual leg spring for three consecutive jumps. Force is normalized by body weight, *i.e.* body mass multiplied by gravitational constant. The spring force (ground reaction force) is estimated based on the acceleration of the hopper's center of mass. Friction forces, which are not accounted for in this estimation, explain the negative force at the end of the upward motion and the onset of the flight phase.

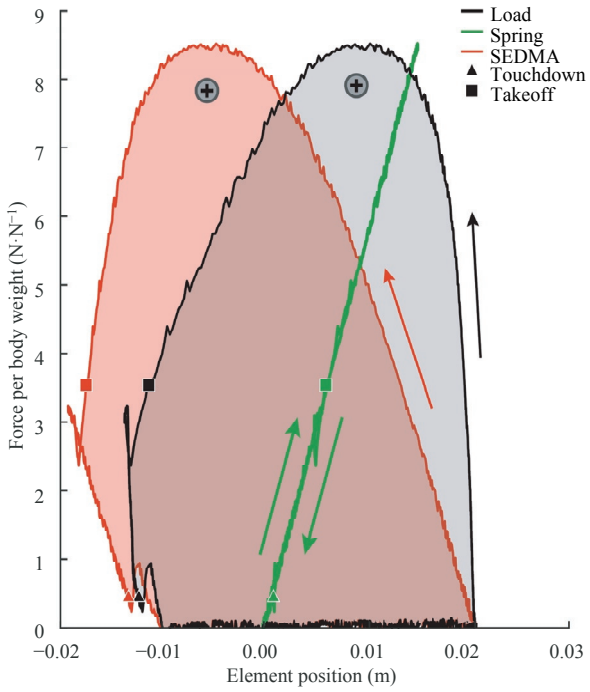

Fig. 6 Workloops of spring (green, estimated from the spring deflection), DMA unit (red) and the entire SEDMA, equivalent to that of the load (black). Force is normalized by body weight, *i.e.* body mass multiplied by gravitational constant).

larger distance than the load side in order to generate the desired cable pull. This shifts the workloop of the SEDMA actuator (red line) to the left.

3.4 Energy-efficiency

Despite the successful implementation of the controller, the energy consumption is surprisingly high. An overview of the hopper's energy and work balances is given in Table 3. For an extensive analysis of the controller's ability to distribute power among the actuators in the most energy-efficient way, we refer to Ref. [32]. Below, we discuss four important components which have an impact on the actuator's energy efficiency: the spring, friction, the inertia of drivetrain components and the resistive losses. As we will discuss in section **4.2**, it is the interplay between these components and losses that leads to a high overall energy consumption.

3.4.1 The role of the spring

The main motivation for the series spring was to protect the mechanical components in the drivetrain – in particular, the gearbox – against shocks during touch-down. But how does the spring affect the hopper's power consumption? The power profiles in Fig. 7 represent the powers on the motor side (*i.e.*, the power delivered by the motor) and the load side of the spring (*i.e.*, the power delivered to the knee). The difference between both is the power absorbed or released by the series spring. Fig. 7 demonstrates the well-known power-enhancing capabilities of the series spring. By storing energy in the spring (2.3 J per cycle), a large part (0.68 J or 30%) already before the start of the upward motion, the work delivered by the drivetrain is spread out over a larger timespan. The result is a reduction of the motor's peak power: a peak of 64 W is delivered to the knee while the drivetrain's output power does not exceed 51 W.

If peak power is reduced by the spring, then what is the explanation for the inefficiency observed in the workloop analysis (section **5.2**)? Fig. 7 reveals that the spring is used somewhat inefficiently during the flight phase (grey area). While the knee power is zero during this phase, the motor power is not. This indicates that some of the energy stored in the spring is not fully converted to work on the hopper, but instead absorbed by the motor, temporarily stored as kinetic energy in drivetrain components, or dissipated as heat by friction.

Furthermore, the hopping frequency of 1.02 Hz is below the antiresonance frequency of the hopper (1.30 Hz). The antiresonance frequency f_{ar} can be derived from the system's equations of motion during the stance phase, by linearizing around a reference angle ϕ_{eq} and imposing a motor angle of zero. This results in the following expression:

$$f_{\text{ar/stance}} = \frac{1}{2\pi}\sqrt{\frac{k_s r_{\text{pulley}}^2 - (2m_H + m_K + 2m_l) g l_l \sin\frac{\phi_{eq}}{2}}{\left[(4m_H + 2m_K)\cos^2\frac{\phi_{eq}}{2} + m_K + \frac{m_l}{3}\right] l_l^2}}, \quad (1)$$

where l_l is the length of a leg link, r_{pulley} is the radius of the knee pulley, k_s is the stiffness of the SEDMA's series spring and m_H, m_K and m_l are the masses of the hip, knee and robot links, respectively. Filling in the system's parameters, specific in section **2**, we find a stance phase antiresonance frequency $f_{\text{ar/stance}}$ = 1.62 Hz. The antiresonance frequency f_{ar} can then be determined by accounting for a flight phase duration of 150 ms, in accordance with the experiments. This results in the value of f_{ar} = 1.30 Hz mentioned above.

Systems with series springs are known to be most energy-efficient at this natural frequency, where motor speed is minimal[43]. In other words, the MARCO Hopper would consume less energy at hopping frequencies higher than f_{ar}, or if the spring stiffness – hence the antiresonance frequency – would be decreased. In Ref. [44], the authors drew similar conclusions from their experiments on a hopping robot with a parallel spring: they found the energy-efficiency of the hopper to be strongly related to its natural (resonance) frequency. At this frequency, theoretically, the knee torque is provided passively by the parallel spring[43].

3.4.2 The role of friction

One of the main advantages of the spring is that it can store the excess gravitational potential energy and kinetic energy in the compression phase (when downward motion takes place). However, Fig. 7 shows that this is not the case for the SEDMA. No power is stored in the spring during the compression phase. In fact, there is no force acting on the spring at all, and the mechanical power is zero on both sides. The cause for this behavior is friction. As can be inferred from the relatively long duration of the compression phase in Fig. 7, the hopper experiences strong damping due to mechanical friction during its downward motion. In experiments where friction compensation was decreased, the hip position did not fall below the position where VMC was initiated, and the hopper got stuck in its extended position.

Despite the impact of the friction experienced by the hopper on the overall energetic performance of the device, its direct contribution to the overall energy is limited (2.94 J or 9.3% out of a total electrical energy consumption of 31.6 J). Friction and other speed-dependent losses in the motor account for a higher percentage of the total energy consumption (10.3 J or 33% of the total energy consumption). This observation is a telling example of how a relatively small amount of friction losses in a mechanical setup can lead to high losses upstream in complex actuators such as the SEDMA, compromising their energy-efficiency.

Table 3 Average estimated energy losses of the Marco II hopper during one hop, normalized by the hopper's total mass (2.723 kg). Friction losses experienced by the hopper (through contact with the ground and sliding of the linear bearings along the vertical rail) are equal to the mechanical energy provided by the knee. Friction losses of the DMA are calculated by means of friction coefficients estimated in Ref. [24]. Transmission losses (gearboxes, spindle, Bowden cable) and losses incurred by the spring make up the rest of the losses.

Parameters	Value ($J \cdot kg^{-1}$)
Friction losses (hopper)	2.94 ± 0.09
Friction losses (motors)	10.3 ± 0.1
Resistive (Joule) losses	4.3 ± 0.1
Electrical energy	31.6 ± 1.7

3.4.3 The role of inertia

All moving components have a certain inertia, which can have a large influence on the resulting power profile. This is especially the case if high gear ratios are used or if the required output acceleration is high[45]. Fig. 8 shows four relevant power flows which can easily be measured. In addition to the electrical power (blue) and the mechanical power available at the output shaft of the DMA (purple), the power stored in the inertia of the drivetrain components (spindle, gearboxes and motors) is plotted in red. The message in this figure is clear: most of the electrical power is used for accelerating the actuator's drivetrain components. In other words, the inertia of the drivetrain is poorly matched with that of the load

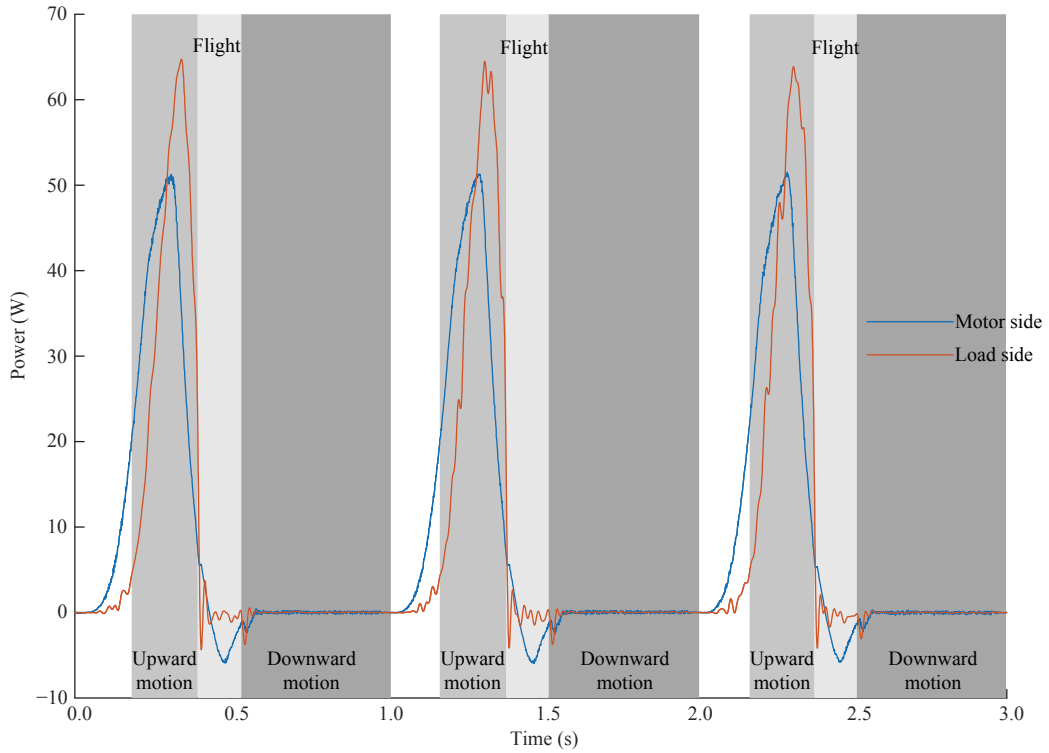

Fig. 7 Power delivered by the motor (blue) and delivered to the knee (red) for three consecutive jumps. The difference between both powers is the power in the spring. Different phases of the hopping motion are denoted by shaded areas. The spring improves the peak power output of the SEDMA.

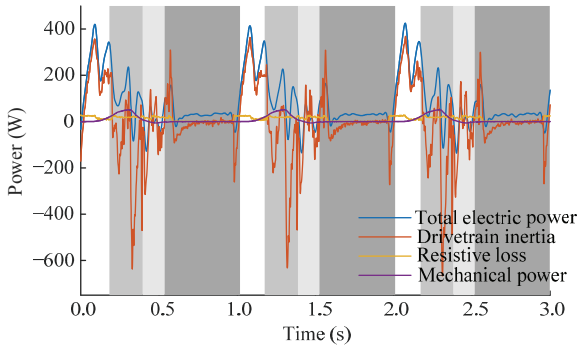

Fig. 8 Power flows for three consecutive jumps. Different phases of the hopping motion are denoted by shaded areas. Inertia is the main power flow in the actuator and strongly determines the electrical power profile. In comparison, the power dissipated as resistive losses in the motors' windings and the power transferred to the load are small.

and the required output accelerations. It is well-known that this can lead to high energy consumption in dynamic applications[46]. The effect can also be seen in Fig. 9, where the position of both ends of the spring (load- and motor side) is shown. During the flight phase, the load-side position remains fairly constant. The motor-side position, however, continues to move due to the inertia of the drivetrain components. The result is a gradual increase in spring length or, in other words, energy being stored in the spring.

3.4.4 The role of resistive losses

Also shown on Fig. 8, in yellow, is the power dissipated in the motors' winding resistance. Compared to the power profile of the drivetrain inertia, resistive losses only account for a minor part of the total electric power, *i.e.* the power measured at the motor terminals. Around 20 W – 25 W is dissipated during upward motion, flight and loading of the spring. Still, in terms of energy consumption, the energy lost through the windings is considerable: around 11.3 J is dissipated as heat, which is more than the energy that is actually transferred to the knee (8.5 J).

4 Discussion

4.1 Biomechanical perspective

The results reveal a number of differences between the actuator-driven leg function and human hopping patterns, but also some similarities. After a brief

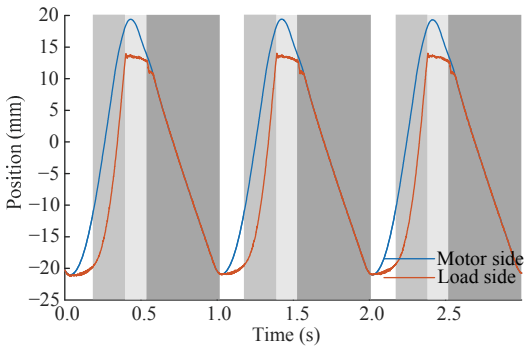

Fig. 9 Positions of both ends of the spring. Different phases of the hopping motion are denoted by shaded areas. The difference between both lines indicates the extension of the spring.

discussion regarding the kinematics and dynamics of both, we explain how these differences and similarities can be related to the design of the leg and the mechanical properties of the setup.

4.1.1 Comparison to human jumping

Most recognizable in the dynamics of the MARCO II hopper was the lack of an eccentric stretching during leg compression. In human jumping, eccentric stretching would store energy in the spring element that can be released during leg extension, resulting in a more efficient jumping performance[14,47]. In the process, the muscles also build up a high level of force before shortening. This enables them to produce more work over the first part of their shortening distance, further enhancing hopping performance[48,49]. In contrast to human hopping, on the Marco Hopper II, no spring extension was generated during the compression phase because the friction of the system (e.g. friction in bearings) dissipated all the energy available from the deceleration of the leg. As a consequence, the robot could not benefit from these energy-saving mechanisms, resulting in a strong increase in its energy consumption.

The force-length relationship, described in section **3.2**, visualized another difference between human and robotic hopping. The relationship of the SEDMA-actuated Marco Hopper II was found to be very non-linear, in contrast to normal human hopping. Interestingly, Farley *et al.*[50] showed that, in humans hopping at lower frequencies, the typical spring-like behavior disappears as well. Instead, the force profile exhibits a peak force midway during the downward motion. The Marco Hopper II displays the exact same behavior, its force-length characteristic having an appearance which is strikingly similar to the ones recorded by Farley *et al.*[50] for low-frequency (1.2 Hz) human hops. There is however no common cause or explanation for this phenomenon. Considering the lack of tension in the Bowden cable, we believe the force peak is caused by position-specific friction in the Marco Hopper II (*e.g.* a defect in the linear bearings), something which is not relevant in human hopping experiments.

While hopping motion does not describe the dynamics of the Marco Hopper II well, squat jumps (*i.e.*, jumps starting from a squatting position) exhibit more similarities. Workloop patterns of leg extensor muscles without eccentric stretching have, for instance, been observed in experimental studies on human squat jumps [14,41,51]. Here, the contractile component of the triceps surae muscle shortened already in the isometric phase (*i.e.*, before plantar flexion of the ankle) giving it more time to do the required work. As such, the contractile component can shorten at a lower and more efficient speed. The same behavior was observed in the Marco Hopper II. As shown in section 3.4.1, the work delivered by the drivetrain is spread out over a larger time span by extending the spring already before the start of the upward motion. In the robotic system, this leads to a reduction of the motor's speed and, consequently, to a lower power requirement.

4.1.2 Influence of the design of the robot

As explained in section **2.2**, the Marco Hopper II was intended as a simplified mechatronic representation of the human leg. Some of the observations presented in this manuscript can be related to this simplified design.

The Marco Hopper II consists of two segments with only one actuated joint, namely the knee joint. In human hopping the main stiffness determinant for hopping at the preferred hopping frequency (around 2.1 Hz) is the ankle joint[52]. This indicates that the design of the Marco Hopper II is not particularly adapted to this type of motion. However, at lower hopping frequencies, the knee becomes relatively more important[53]. It therefore makes more sense to study low-frequency jumping motions on this setup.

Furthermore, in biomechanics, the coupling of the ankle and knee joint through the biarticular Gastrocne-

mius (GAS) muscle plays an important role in synchronizing the knee and ankle joints and in redirecting the kinetic energy of the deaccelerating shank and thigh segments to the ankle joint during the last phase of push off[15,54,55]. With GAS, the knee joint can be fully extended in preparation of take-off. The high rotational energy in thigh and shank can be transferred by the GAS to an extension of ankle joint. As the foot is about perpendicular to leg axis, it translates the energy transferred by the GAS to foot extension and, consequently, to leg extension. Here, only small energy losses will occur due to rotational energy in the lightweight foot (mass of around 1 kg).

While the Marco Hopper II misses these structures, the acceleration of the foot was achieved through a mechanical end stop (knee stop), implemented as a steel string. When the hip is accelerated upwards, the foot remains on the ground until the string, which is slack during leg compression, prevents the knee from extending above 165°. As a consequence, the resultant impulse accelerates the foot segment vertically. The end stop limit thus defines the take-off and landing posture of the leg limiting the range of motion of the knee and consequently the range in which the hip segment can be accelerated (during the extension phase). An increased knee angle at take-off would therefore result in an improved hopping performance. Compared to human hopping, the mechanical knee end stop did not represent an almost fully extended knee (around 175°) at takeoff[15,56].

Finally, there is the zig-zag architecture of the human body, which allows to negotiate the forward and backward accelerations of the body segments during the stance phase of hopping[57]. This is different to the Marco II robot, where the leg segments will accelerate backward during the second half of ground contact. This translational energy is not used for upward acceleration of the body, making the overall motion less efficient. An extension of the robot with a trunk and a foot segment could resolve this issue.

4.2 Technical perspective

While the SEDMA and its controller succeeded in its main goal of generating a repeatable hopping pattern, its performance-enhancing capabilities remained mostly unexploited in the tests. The design process of the SEDMA involves the proper selection of the series spring stiffness and the optimal composition of the redundant drivetrain (DMA) – two design challenges which are the subject of ongoing research[24,25,43,44].

We identified several aspects which are crucial for the mechanical design of high-performing hopping machines with elastic-redundant actuators. Firstly, friction needs to be avoided at all costs in spring-enhanced drivetrains, as it reduces the amount of energy which can be stored and re-injected by the spring. Secondly, a less appropriate selection of the spring constant will complicate the excitation of the natural dynamics of hopping. Finally, although the motions of the composing drivetrains of the redundant actuator can be optimized in control, sizing their components to the task at hand still remains important. This was a relevant problem for the SEDMA studied in this work. Initially designed for high-torque operation in steady-state conditions[24], the DMA's reflected inertia was relatively high for the dynamic hopping task in this work. To mitigate this problem, a series spring was inserted into the drivetrain. In such an arrangement, the spring reduces the speed requirement and, consequently, the acceleration required from the motor, enabling the SEDMA to operate at higher frequencies. However, because friction prevented the spring from storing a reasonable amount of energy, the series spring did not fulfill this function. As a result, high accelerations were demanded of the DMA's motors, so that a large fraction of their input torques was needed to accelerate their own inertia. This strongly reduced the torque that could be transferred to the hopper and, ultimately, limited the hopping frequency to suboptimal values (*i.e.* below the antiresonance frequency).

The results presented in this paper demonstrate that traditional design strategies fall short when applied to complex actuators combining elastic elements with redundant motors. One of the main issues is dealing with unpredictable deviations from the expected task requirements, such as friction. When sizing servomotors, one anticipates friction by oversizing the drivetrain by a small margin. In the SEDMA, however, the effect of friction can be amplified through the interplay of the elastic element and the redundant motors. If the level of friction is significant, as was the case in our experiments,

this can result in a surprisingly strong decrease in performance of the actuator. We expect that the actuator's versatility granted by its redundant degrees of freedom[28] could be utilized to mitigate this problem. This would, however, require novel control and design strategies capable of dealing with the redundancy of the system, the interplay of the motors with the elastic element and the impact of uncertain loads. At present, this complex problem forms a bottleneck for the adoption of elastic-redundant actuation concepts in robotics.

5 Conclusion

In this paper, we discussed and investigated how the principles of redundancy and series elastic actuation can be combined in bio-inspired robots. We focused on kinematic redundancy on a motor level which, in humans, is found at the myofibril level, one of the deepest levels of construction of the human muscle. With the goal of studying the potential of this actuation principle for bioinspired motion, we presented a hopping robot actuated by the kinematically redundant SEDMA. Experiments showed that the actuator was able to generate consistent jumps at low frequency, resembling human squat jumps.

We argue that bio-inspired designs incorporating series compliance and redundant actuation provide a high potential for efficiency improvements in human-like motions. However, the design and control of such actuators is strongly complicated by their large number of parameters as well as the complex dynamics induced by the redundant drivetrains and the compliant element. Typically, this issue is resolved by relying heavily on known information regarding the motion task. In this regard, friction – which is hard to model and quantify a priori – poses a relevant problem. In the hopping motions studied in this paper, high levels of friction prevented energy storage in the compliant element of the SEDMA. This drastic change in the dynamics of the motion task and, therefore, in the actuator requirements, resulted in hopping frequencies below the expected values. We conclude that, although complicated, it is of utmost importance to anticipate uncertainty in the specific demands of the motion task during the mechanical and control design of an actuator combining redundancy and elasticity. Further research in this direction is thus needed to exploit the full potential of this class of actuators.

Acknowledgment

Tom Verstraten is a postdoctoral fellow of the Research Foundation Flanders - Fonds voor Wetenschappelijk Onderzoek (FWO). Part of this work was funded by the European Commission starting grant SPEAR (no. 337596) and the DFG grants BE 5729/2 and BE 5729/1. We would like to thank Rustam Galljamov and Philipp Overath for their assistance with the demonstrator and the experiments.

* All supplementary materials are available at https://doi.org/10.1007/s42235-020-0062-z.

References

[1] Raibert M H. *Legged Robots That Balance*, MIT press, Cambridge, MA, USA, 1986.

[2] Sayyad A, Seth B, Seshu P. Single-legged hopping robotics research – A review. *Robotica*, 2007, **25**, 587–613.

[3] Zhang Z Q, Zhao J, Chen H L, Chen D S. A survey of bioinspired jumping robot: Takeoff, air posture adjustment, and landing buffer. *Applied Bionics and Biomechanics*, **2017**, 2017, 22.

[4] Full R J, Koditschek D E. Templates and anchors: Neuromechanical hypotheses of legged locomotion on land. *The Journal of Experimental Biology*, 1999, **202**, 3325–3332.

[5] Blickhan R. The spring-mass model for running and hopping. *Journal of Biomechanics*, 1989, **22**, 1217–1227.

[6] Sharbafi M A, Seyfarth A, Zhao G. Locomotor sub-functions for control of assistive wearable robots. *Frontiers in Neurorobotics*, 2017, **11**, 44.

[7] Haldane D W, Plecnik M M, Yim J K, Fearing R S. Robotic vertical jumping agility *via* series-elastic power modulation. *Science Robotics*, 2016, **1**, eaag2048.

[8] Sato A, Buehler M. A planar hopping robot with one actuator: Design, simulation, and experimental results. *Proceedings of the IEEE/RSJ International Conference on Intelligent Robots and Systems* (*IROS*), Sendai, Japan, 2004, 3540–3545.

[9] Batts Z, Kim J, Yamane K. Design of a hopping mechanism using a voice coil actuator: Linear elastic actuator in parallel (LEAP). *Proceedings of the IEEE International Conference on Robotics and Automation* (*ICRA*), Stockholm, Sweden, 2016, 655–660.

[10] Liu X, Poulakakis I. On the energetics of a switchable

parallel elastic actuator design for monopedal running. *Proceedings of the IEEE International Conference on Robotics and Biomimetics* (*ROBIO*), Zhuhai, China, 2015, 769–774.

[11] Alexander R McN. Three uses for springs in legged locomotion. *The International Journal of Robotics Research*, 1990, **9**, 53–61.

[12] Lichtwark G A, Wilson A M. *In vivo* mechanical properties of the human Achilles tendon during one-legged hopping. *The Journal of Experimental Biology*, 2005, **208**, 4715–4725.

[13] Biewener A A, Konieczynski D D, Baudinette R V. *In vivo* muscle force-length behavior during steady-speed hopping in tammar wallabies. *The Journal of Experimental Biology*, 1998, **201**, 1681–1694.

[14] Anderson F C, Pandy M G. Storage and utilization of elastic strain energy during jumping. *Journal of Biomechanics*, 1993, **26**, 1413–1427.

[15] Bobbert M F, Huijing P A, van Ingen Schenau G J. An estimation of power output and work done by the human triceps surae musle – Tendon complex in jumping. *Journal of Biomechanics*, 1986, **19**, 899–906.

[16] Ontañón-Ruiz J, Daniel R W, McĂree P R. On the use of differential drives for overcoming transmission nonlinearities. *Journal of Robotic Systems*, 1998, **15**, 641–660.

[17] Lee H, Choi Y. A new actuator system using dual-motors and a planetary gear. *IEEE/ASME Transactions on Mechatronics*, 2012, **17**, 192–197.

[18] Girard A, Asada H H. Leveraging natural load dynamics with variable gear-ratio actuators. *IEEE Robotics and Automation Letters*, 2017, **2**, 741–748.

[19] Siciliano B, Khatib O. *Springer Handbook of Robotics*, 1st ed, Springer-Verlag, Berlin Heidelberg, Germany, 2008.

[20] Field G, Stepanenko Y. Iterative dynamic programming: an approach to minimum energy trajectory planning for robotic manipulators. *Proceedings of the IEEE International Conference on Robotics and Automation*, Minneapolis, MN, USA, 1996, 2755–2760.

[21] von Stryk O, Schlemmer M. Optimal control of the industrial robot manutec r3. In: *Computational Optimal Control*, Bulirsch R and Kraft D eds., Birkhäuser Basel, Basel, Switzerland, 1994, 367–382.

[22] Nenchev D N. Redundancy resolution through local optimization: A review. *Journal of Robotic Systems*, 1989, **6**, 769–798.

[23] Mathijssen G, Furnémont R, Verstraten T, Brackx V, Premec J, Jiménez R, Lefeber D, Vanderborght B. +SPEA introduction: Drastic actuator energy requirement reduction by symbiosis of parallel motors, springs and locking mechanisms. *Proceedings of the IEEE International Conference on Robotics and Automation* (*ICRA)*, Stockholm, Sweden, 2016, 676–681.

[24] Verstraten T, Furnémont R, Lopez-Garcia P, Rodriguez-Cianca D, Cao H L, Vanderborght B, Lefeber D. Modeling and design of an energy-efficient dual-motor actuation unit with a planetary differential and holding brakes. *Mechatronics*, 2018, **49**, 134–148.

[25] Rabindran D, Tesar D. Parametric design and power-flow analysis of parallel force/velocity actuators. *Journal of Mechanisms and Robotics*, 2009, **1**, 011007.

[26] Rabindran D, Tesar D. Study of the dynamic coupling term (μ) in parallel force/velocity actuated systems. *Proceedings of the IEEE International Conference on Automation Science and Engineering*, Scottsdale, AZ, USA, 2007, 418–423.

[27] Kim B S, Park J J, Song J B. Improved manipulation efficiency using a serial-type dual actuator unit. *Proceedings of the International Conference on Control*, *Automation and Systems* (*ICCAS*), Seoul, Korea, 2007, 30–35.

[28] Verstraten T, Furnémont R, López-García P, Rodriguez-Cianca D, Vanderborght B, Lefeber D. Kinematically redundant actuators, a solution for conflicting torque-speed requirements. *The International Journal of Robotics Research*, 2019, **38**, 612–629.

[29] Rabindran D, Tesar D. A differential-based dual actuator for a safe robot joint: Theory and experiments. *Proceedings of the World Automation Congress* (*WAC*), Waikoloa, HI, USA, 2014, 142–147.

[30] Verstraten T, Furnémont R, López-García P, Crispel S, Vanderborght B, Lefeber D. A series elastic dual-motor actuator concept for wearable robotics. *Proceedings of the* 4*th International Symposium on Wearable Robotics* (*WeRob*2018), Pisa, Italy, 2018, 165–169.

[31] Pratt J, Chew C M, Torres A, Dilworth P, Pratt G. Virtual model control: An intuitive approach for bipedal locomotion. *The International Journal of Robotics Research*, 2001, **20**, 129–143.

[32] Verstraten T, Furnémont R, Beckerle P, Vanderborght B, Lefeber D. A hopping robot driven by a series elastic dual-motor actuator. *IEEE Robotics and Automation Letters*, 2019, **4**, 2310–2316.

[33] Hoffmann M, Simanek J. The merits of passive compliant joints in legged locomotion: Fast learning, superior energy

efficiency and versatile sensing in a quadruped robot. *Journal of Bionic Engineering*, 2017, **14**, 1–14.

[34] Kajita S, Nagasaki T, Kaneko K, Yokoi K, Tanie K. A running controller of humanoid biped HRP-2LR. *Proceedings of the IEEE International Conference on Robotics and Automation*, Barcelona, Spain, 2005, 616–622.

[35] Oehlke J, Sharbafi M A, Beckerle P, Seyfarth A. Template-based hopping control of a bio-inspired segmented robotic leg. *Proceedings of the 6th IEEE International Conference on Biomedical Robotics and Biomechatronics* (*BioRob*), Singapore, Singapore, 2016, 35–40.

[36] Winter D A. *Biomechanics and Motor Control of Human Movement*, 4th ed, John Wiley & Sons, Hoboken, NJ, USA, 2009.

[37] Oehlke J, Beckerle P, Seyfarth A, Sharbafi M A. Human-like hopping in machines. *Biological Cybernetics*, 2019, **113**, 227–238.

[38] Guo W, Cai C R, Li M T, Zha F S, Wang P F, Wang K N. A parallel actuated pantograph leg for high-speed locomotion. *Journal of Bionic Engineering*, 2017, **14**, 202–217.

[39] Seyfarth A, Blickhan R , Van Leeuwen J L. Optimum take-off techniques and muscle design for long jump. *Journal of Experimental Biology*, 2000, **203**, 741–750.

[40] Seyfarth A, Friedrichs A, Wank V, Blickhan R. Dynamics of the long jump. *Journal of Biomechanics*, 1999, **32**, 1259–1267.

[41] Finni T, Komi P V, Lepola V. *In vivo* human triceps surae and quadriceps femoris muscle function in a squat jump and counter movement jump. *European Journal of Applied Physiology*, 2000, **83**, 416–426.

[42] Schumacher C, Seyfarth A. Sensor-motor maps for describing linear reflex composition in hopping. *Frontiers in Computational Neuroscience*, 2017, **11**, 108.

[43] Verstraten T, Beckerle P, Furnémont R, Mathijssen G, Vanderborght B, Lefeber D. Series and parallel elastic actuation: Impact of natural dynamics on power and energy consumption. *Mechanism and Machine Theory*, 2016, **102**, 232–246.

[44] Vu H Q, Yu X X, Iida F, Pfeifer R. Improving energy efficiency of hopping locomotion by using a variable stiffness actuator. *IEEE/ASME Transactions on Mechatronics*, 2016, **21**, 472–486.

[45] Verstraten T, Furnémont R, Mathijssen G, Vanderborght B, Lefeber D. Energy consumption of geared DC motors in dynamic applications: Comparing modeling approaches. *IEEE Robotics and Automation Letters*, 2016, **1**, 524–530.

[46] Verstraten T, Mathijssen G, Furnémont R, Vanderborght B, Lefeber D. Modeling and design of geared DC motors for energy efficiency: Comparison between theory and experiments. *Mechatronics*, 2015, **30**, 198–213.

[47] Cavagna G A. Storage and utilization of elastic energy in skeletal muscle. *Exercise and Sport Sciences Reviews*, 1977, **5**, 89–130.

[48] Bobbert M F, Gerritsen K G M, Litjens M C A, Van Soest A J. Why is countermovement jump height greater than squat jump height? *Medicine & Science in Sports & Exercise,* 1996, **28**, 1402–1412.

[49] Bobbert M F, Mackay M, Schinkelshoek D, Huijing P A, van Ingen Schenau G J. Biomechanical analysis of drop and countermovement jumps. *European Journal of Applied Physiology and Occupational Physiology*, 1986, **54**, 566–573.

[50] Farley C T, Blickhan R, Saito J, Taylor C R. Hopping frequency in humans: A test of how springs set stride frequency in bouncing gaits. *Journal of Applied Physiology*, 1991, **71**, 2127–2132.

[51] Kawakami Y, Muraoka T, Ito S, Kanehisa H, Fukunaga T. *In vivo* muscle fibre behaviour during counter-movement exercise in humans reveals a significant role for tendon elasticity. *The Journal of Physiology*, 2002, **540**, 635–646.

[52] Farley C T, Morgenroth D C. Leg stiffness primarily depends on ankle stiffness during human hopping. *Journal of Biomechanics*, 1999, **32**, 267–273.

[53] Hobara H, Inoue K, Omuro K, Muraoka T, Kanosue K. Determinant of leg stiffness during hopping is frequency-dependent. *European Journal of Applied Physiology*, 2011, **111**, 2195–2201.

[54] Prilutsky B I, Zatsiorsky V M. Tendon action of two-joint muscles: Transfer of mechanical energy between joints during jumping, landing, and running. *Journal of Biomechanics*, 1994, **27**, 25–34.

[55] Junius K, Moltedo M, Cherelle P, Rodriguez-Guerrero C, Vanderborght B, Lefeber D. Biarticular elements as a contributor to energy efficiency: Biomechanical review and application in bio-inspired robotics. *Bioinspiration & Biomimetics*, 2017, **12**, 061001.

[56] Bobbert M F, Richard Casius L J. Spring-like leg behaviour, musculoskeletal mechanics and control in maximum and submaximum height human hopping. *Philosophical Transactions of the Royal Society B*: *Biological Sciences*, 2011, **366**, 1516–1529.

[57] Seyfarth A, Günther M, Blickhan R. Stable operation of an elastic three-segment leg. *Biological Cybernetics*, 2001, **84**, 365–382.